

Synthesis of 9,9-Bis(4-aminophenyl)fluorene-Based Benzoxazine and Properties of Its High-Performance Thermoset

Hou Chien Chang,¹ Ching Hsuan Lin,¹ Yu Wei Tian,¹ Yu Ren Feng,¹ Li Hsin Chan²

¹Department of Chemical Engineering, National Chung Hsing University, Taichung 402, Taiwan

²Department of Applied Materials and Optoelectronic Engineering, National Chi Nan University, Puli, Taiwan

Correspondence to: C. H. Lin (E-mail: lynch@nchu.edu.tw)

Received 4 November 2011; accepted 22 December 2011; published online 28 February 2012

DOI: 10.1002/pola.25993

ABSTRACT: A benzoxazine (**P-bapf**) based on 9,9-bis(4-aminophenyl)fluorene (BAPF), phenol, and formaldehyde was successfully prepared using two-pot and one-pot procedures. In the two-pot approach, BAPF initially reacted with 2-hydroxybenzaldehyde, leading to 9,9-bis(4-(2-hydroxybenzylideneimino)phenyl)fluorene. The imine linkages of 9,9-bis(4-(2-hydroxybenzylideneimino)phenyl)fluorene were then reduced by sodium borohydride, forming 9,9-bis(4-(2-hydroxybenzylamino)phenyl)fluorene. Finally, paraformaldehyde was added to induce ring closure condensation, forming benzoxazine (**P-bapf**). In the one-pot approach, **P-bapf** was obtained directly by reacting BAPF, phenol, and paraformaldehyde in various solvents. Among the solvents, we found that using toluene/ethanol (2/1, v/v) as a solvent leads to the best purity and yield. No gelation was observed in the preparation. The struc-

ture of the resulting benzoxazine was confirmed by ¹H, ¹³C, ¹H-¹H and ¹H-¹³C NMR spectra. **P-bapf** exhibits a photoluminescent emission at 395 nm under an excitation of 275 nm. After curing, the resulting **P-bapf** thermoset exhibits *T_g* as high as 236 °C, and the *T_g* can be further increased to 260 °C by copolymerization with an equal equivalent of cresol novolac epoxy. The 5% degradation temperature of the **P-bapf** thermoset reaches as high as 413 °C (N₂) and 431 °C (air). The refractive index at 589 nm is as high as 1.70, demonstrating a high refractive index characteristic of fluorene linkage. © 2012 Wiley Periodicals, Inc. *J Polym Sci Part A: Polym Chem* 50: 2201–2210, 2012

KEYWORDS: thermosets; ring-opening polymerization; refractive index

INTRODUCTION Benzoxazines are resins that can be polymerized to thermosets by means of thermally activated ring-opening reactions.¹ Thermosets with low water absorption, superior electrical properties,² and low surface energy³ can be obtained after curing. Benzoxazines can be monofunctional, difunctional, or multifunctional. Among them, difunctional benzoxazines have received the most attention due to their balanced processability and thermal properties after curing. There are two types of difunctional benzoxazines, including bisphenol-based benzoxazines and diamine-based benzoxazines (Fig. 1). Bisphenol-based benzoxazines are prepared by the condensation of bisphenol, primary monoamine, and formaldehyde [Fig. 1(a)]. The wide variety of aromatic bisphenols and monoamines allow for the considerable molecule-design flexibility of benzoxazines. Some special functional groups, such as acetylene,^{4,5} furan,⁶ allyl,⁷ propargyl,⁸ maleimide,⁹ carboxylic acid,¹⁰ methacryloyl,¹¹ and amine¹² have been incorporated into benzoxazines to provide some desired properties. Diamine-based benzoxazines are prepared by the condensation of diamine, formaldehyde, and monophenol [Fig. 1(b)]. Unlike bisphenol-based benzoxa-

zines, aromatic diamine-based benzoxazines have rarely been using a one-pot procedure.^{12–15} In addition, to the best of our knowledge, most reported diamine-based benzoxazines prepared using the one-pot procedure have generally been based on diaminodiphenylmethane, although benzoxazine based on diaminodiphenylsulfone has also been reported.¹³ Recently, we proposed a three-step procedure to prepare aromatic diamine-based benzoxazines.^{16,17} Almost simultaneously, Ronda and coworker prepared deuterated benzoxazines to prove the mechanism.¹⁸ Endo and coworkers also applied a similar approach to prepare poly(allylamine)-based benzoxazine.¹⁹ Liu and coworkers used the same approach to prepare phosphazine-containing benzoxazines.^{20,21} Although the approach is time consuming, it can be applied in preparing various diamine or multifunctional amine-based benzoxazines.

The fluorene group contains two benzene rings that are connected via a carbon–carbon bond and an adjacent methylene bridge.²² The methylene bridge forces the two phenyl rings to be planar, thereby providing high overlaps of

Additional Supporting Information may be found in the online version of this article.

© 2012 Wiley Periodicals, Inc.

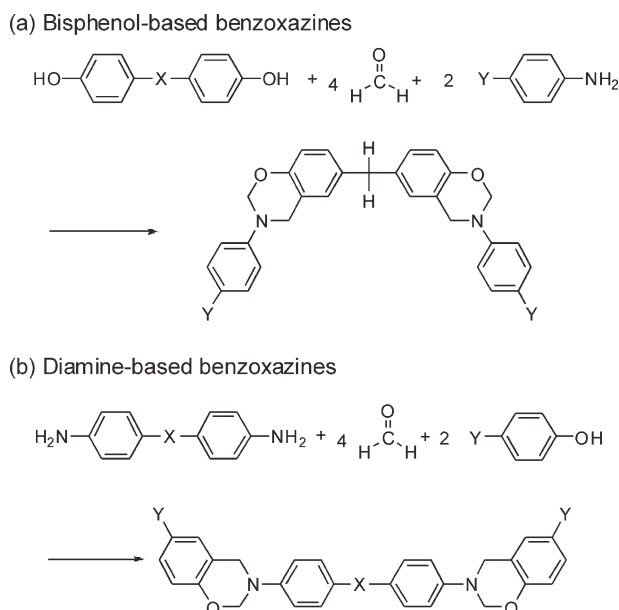


FIGURE 1 Synthesis of (a) bisphenol-based and (b) diamine-based benzoxazines.

π orbitals. Fluorene-based conjugated polymers have received much attention in polymer light-emitting diodes.^{23,24} 9,9-Bis(4-hydroxyphenyl)fluorene (BHPF) has two phenol linkages at the bridge position of fluorene. The four phenyl rings of BHPF are connected to a quaternary carbon, leading to a severe rotational hindrance of the phenyl rings. Therefore, incorporating the rigid and bulky fluorenyl moiety to polymers leads to enhanced thermal properties, solubility, and refractive index.^{25–27} Recently, Liu and coworkers prepared fluorene-containing benzoxazines based on BHPF, primary amines, and formaldehyde.²⁸ The fluorene-based polybenzoxazines show remarkably higher T_g and better thermal stability than the thermoset of B-a, which is a benzoxazine based on bisphenol A, aniline, and formaldehyde. Liu et al. prepared fluorene-containing benzoxazine based on BHPF, furfurylamine, and formaldehyde.²⁹ The resulting polybenzoxazine exhibits high T_g , high modulus, good thermal stability, and a high refractive index. In addition, the resulting benzoxazine displays high photoluminescent intensity in the blue-light band.

9,9-Bis(4-aminophenyl)fluorene (BAPF) has a similar structure to BHPF except that the hydroxyl moiety is replaced by aniline moiety. Because of the unusual rotational hindrance of the four phenyl rings, BAPF and its derivatives have been used in polyimides,^{30,31} sulfonated polyimides,³² polyimine,³³ and epoxy.³⁴ In our previous paper, we reported that diamine-based polybenzoxazines exhibited better thermal stability than biphenol-based polybenzoxazines. For example, thermoset of diaminodiphenylmethane-based benzoxazine (**P-ddm**) exhibits 53 °C higher in T_g , and 120 °C higher in 5 wt % decomposition temperature than the thermoset of bisphenol F-based benzoxazine (F-a), although **P-ddm** and F-a are constitutional isomers.¹⁶ Therefore, it would be interesting to prepare a BAPF-based polybenzoxazine and compare its

properties with those of BHPF-based polybenzoxazines. In this work, we use two approaches to prepare a benzoxazine (**P-bapf**) based on BAPF, phenol, and formaldehyde. The first is a two-pot procedure based on a modified procedure of our previous work,^{16,17} and the second is a one-pot procedure using a special cosolvent. The resulting BAPF-based benzoxazine displays a photoluminescent peak at 395 nm. The resulting polybenzoxazine shows T_g as high as 236 °C, a coefficient of thermal expansion as low as 36 ppm/°C, and 5% degradation temperature as high as 416 °C (N₂), and 431 °C (air). The refractive index is as high as 1.70 (589 nm). Detailed synthesis and properties of the resulting thermosets are provided in this work.

EXPERIMENTAL

Materials

BAPF (from TCI), paraformaldehyde (from TCI), 2-hydroxybenzaldehyde (from Showa), and sodium borohydride (NaBH₄, from Acros) were used as received. Cresol novolac epoxy (CNE) with epoxy equivalent weight 200 g/equiv. was kindly supplied by Chang Chun Plastics, Taiwan under the trade name CNE-200ELD. *N,N*-Dimethylacetamide (DMAc) was purchased from TEDIA, purified by distillation under reduced pressure over calcium hydride (from Acros), and stored over molecular sieves. 1,4-Dioxane, toluene, xylene, chloroform, and ethanol (99.5%) were purchased from TEDIA and used without further purification.

Characterization

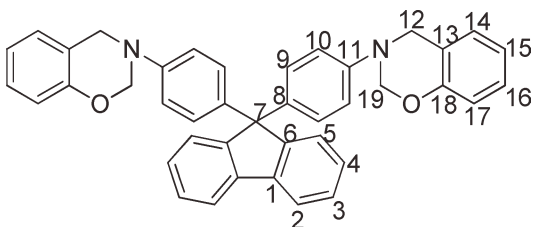
Differential scanning calorimetry (DSC) scans were obtained using a Perkin-Elmer DSC 7 in a nitrogen atmosphere at a heating rate of 20 °C/min. Thermal gravimetric analysis (TGA) was performed with a Perkin-Elmer Pyris1 at a heating rate of 20 °C/min in an atmosphere of nitrogen or air. Dynamic mechanical analysis (DMA) was performed with a Perkin-Elmer Pyris Diamond DMA with a sample size of 5.0 cm × 1.0 cm × 0.2 cm. The storage modulus E' and tan δ were determined as the sample was subjected to the temperature scan mode at a programmed heating rate of 5 °C/min at a frequency of 1 Hz. The test was performed by a bending mode with an amplitude of 5 μ m. Thermal mechanical analysis (TMA) was performed with a Perkin-Elmer Pyris Diamond TMA at a heating rate of 5 °C/min. NMR measurements were performed using a Varian Inova 600 NMR in DMSO-*d*₆, and the chemical shift was calibrated by setting the chemical shift of DMSO-*d*₆ as 2.49 ppm. IR Spectra were obtained from at least 32 scans in the standard wavenumber range of 400–4000 cm⁻¹ using a Perkin-Elmer RX1 infrared spectrophotometer. UV-vis spectra were recorded with a Varian Cary 50 in the standard wavenumber range of 200–800 cm⁻¹. Photoluminescence spectra were measured on a Hitach4500 fluorescence spectrophotometer at a concentration of 10⁻⁵ M. The excitation wavelength is 275 nm. Refractive index was obtained by an ellipsometer SOPRA, GES-5E.

Two-Pot Synthesis of BAPF-Based Benzoxazine

In the first procedure of this approach, 2-hydroxybenzaldehyde 3.68 g (30.13 mmol), BAPF 5.00 g (14.35 mmol), and DMAc/toluene (2/1, v/v) 45 mL were introduced into a

100-mL glass flask equipped with a nitrogen inlet, a magnetic stirrer, and a Dean–Stark trap. The reaction mixture was stirred at reflux temperature for 12 h. After the reaction solution was cooled to room temperature, NaBH₄ 1.74 g (45.92 mmol) was added, and the reaction mixture was stirred for an additional 12 h at room temperature. The mixture was then poured into water. The precipitate was filtrated and then dried in a vacuum oven. Yellow powder (88% yield) was obtained. In the second procedure of this approach, (2) 5.0 g (8.90 mmol), paraformaldehyde 0.84 g (28.6 mmol), and chloroform 100 mL were introduced into a 250-mL glass flask equipped with a nitrogen inlet, a condenser, and a magnetic stirrer. The mixture was stirred at reflux temperature for 8 h. After that, the solution was poured into *n*-hexane. The precipitate was filtrated and then dried in a vacuum oven. Light yellow powder (85% yield) was obtained.

¹H NMR (DMSO-*d*₆), δ = 4.60 (2H, H¹²), 5.40 (2H, H¹⁹), 6.70 (2H, H¹⁷), 6.82 (2H, H¹⁵), 6.90–7.0 (4H, H⁹, H¹⁰), 7.06 (2H, H¹⁴, H¹⁶), 7.24 (2H, H⁴), 7.30–7.40 (4H, H³, H⁵). ¹³C NMR (DMSO-*d*₆), δ = ¹³C NMR (DMSO-*d*₆), δ = 116.3 (C¹⁷), 117.1 (C⁹), 120–121 (C¹³, C¹⁵), 121.5 (C²), 126.0 (C³), 127.1–128.7 (C⁴, C⁵, C¹⁴, C¹⁶), 128.3 (C¹⁰), 137.5 (C⁸), 139.3 (C⁶), 146.2 (C¹), 151 (C¹¹), 154 (C¹⁸). ELEM. ANAL: calculated C, 84.22%; H, 5.52%; N, 4.79% for C₄₁H₃₂N₂O₂ Found C, 84.10%; H, 5.62%; N, 4.70%. FTIR (KBr): 945 cm⁻¹ (N–C–O stretch), 1039 cm⁻¹ (Ar–O–C symmetric stretch), 1223 cm⁻¹ (Ar–O–C asymmetric stretch), 1377 cm⁻¹ (C–N stretch). The BAPF-based benzoxazine prepared using this two-pot procedure is referred to as **P-bapf-2**.

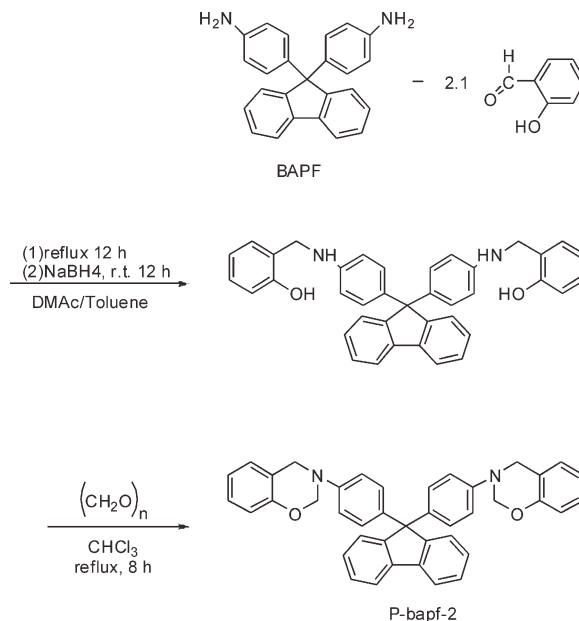


One-Pot Synthesis of BAPF-Based Benzoxazine

BAPF 5.0 g (92.45 mmol), phenol 2.71 g (184.9 mmol), paraformaldehyde 1.72 g (57.4 mmol), and a mixed solvent of toluene/ethanol 150 mL (2/1, v/v) were introduced into a round-bottomed 250-mL glass flask equipped with a nitrogen inlet, a condenser, and a magnetic stirrer. The reaction mixture was stirred at 80 °C for 12 h. After that, the solution was poured into *n*-hexane. The precipitate was filtered and then dried in a vacuum oven. Yellow powder (65% yield) was obtained. ELEM. ANAL: calculated C, 84.22%; H, 5.52%; N, 4.79% for C₄₁H₃₂N₂O₂ Found C, 83.98%; H, 5.72%; N, 4.69%. The BAPF-based benzoxazine prepared using this one-pot procedure is referred to as **P-bapf-1**.

Preparation of Polybenzoxazines

As **P-bapf-2** has better purity than **P-bapf-1** (as discussed later), the curing of benzoxazine was based on **P-bapf-2**. The UV-vis, photoluminescence (PL), and IR analysis are all based on **P-bapf-2**. In the curing process, **P-bapf-2** was initially stirred at 160 °C in an aluminum mold and then cured



SCHEME 1 Synthesis of **P-bapf-2**.

for 2 h at each of 180, 200, and 220 °C in an air-circulating oven. Thereafter, samples were allowed to cool slowly to room temperature to prevent cracking. For **P-bapf** and CNE copolymer, mixtures of (**P-bapf-2**)/CNE with equal equivalency were melted, stirred, and transferred to an aluminum mold and then cured under the same condition used for as **P-bapf-2**.

RESULTS AND DISCUSSION

Two-Pot Synthesis of BAPF-Based Benzoxazine

The BAPF-based benzoxazine was successfully synthesized using a modified two-pot procedure.^{16,17} The resulting benzoxazine is referred to as **P-bapf-2**. In the first procedure of this approach, 2-hydroxybenzaldehyde reacted with BAPF, yielding an intermediate with an *o*-hydroxyl phenylimine linkage. Sodium borohydride was then used to reduce the imine linkage, yielding 9,9-bis(4-(2-hydroxybenzylamino))fluorene. In the second pot, paraformaldehyde was added to the chloroform solution of 9,9-bis(4-(2-hydroxybenzylamino)phenyl)fluorene to induce ring closure condensation, forming **P-bapf-2** (Scheme 1).

Figure 2 shows the ¹H NMR spectrum of **P-bapf-2**. The characteristic peaks of benzoxazines, O–CH₂–N, and ph–CH₂–N at 5.4 and 4.6 ppm confirm the structure of benzoxazines. No signal was observed at around 4.0 ppm corresponding to the N–CH₂–ph as a result of the ring opening of benzoxazine, revealing the purity of the synthesized benzoxazine.

Figure 3 shows the ¹³C NMR spectra of **P-bapf-2**. The characteristic peaks of benzoxazines, O–CH₂–N, and ph–CH₂–N, at 48.9 and 78.5 ppm confirm the structure of benzoxazines. The detailed assignment of each peak in Figures 2 and 3, assisted by the correlation in ¹H–¹H and ¹H–¹³C spectra (Figs. S1 and S2, Supporting Information), confirms the structure of **P-bapf-2**.

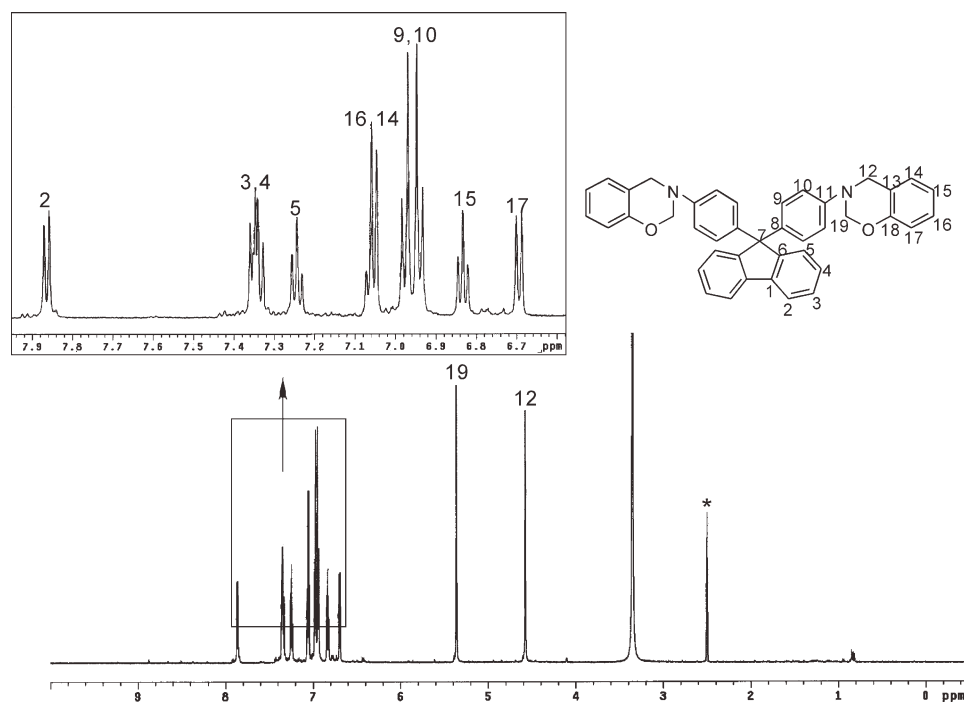


FIGURE 2 ^1H NMR spectrum of P-bapf-2 in $\text{DMSO-}d_6$.

One-Pot Synthesis of BAPF-Based Benzoxazine

According to the literature, synthesis of bisphenol-based benzoxazine can be divided into two steps: the formation of triazine and the dissociation of the resulting triazine.³⁵ Based on this knowledge, the diamine-based benzoxazine is expected to proceed according to the similar steps. The first step involves the formation of a triazine network (R_1), and the second step is the dissociation of the resulting triazine network (R_2 ; Scheme 2). Note that a network will be formed

because diamine and formaldehyde are tetrafunctional and difunctional, respectively. In our previous work involved with the preparation of diamine/bisphenol A/formaldehyde-based polybenzoxazines,³⁶ we proposed that competition between R_1 and R_2 plays a key role in polybenzoxazine synthesis. If $R_1 \gg R_2$, gelation will occur. On the other hand, if $R_1 < R_2$, a soluble product will be produced. In that work, we found that toluene/ethanol (2/1, v/v) is an effective cosolvent in reducing R_1 . Based on the finding, we examine

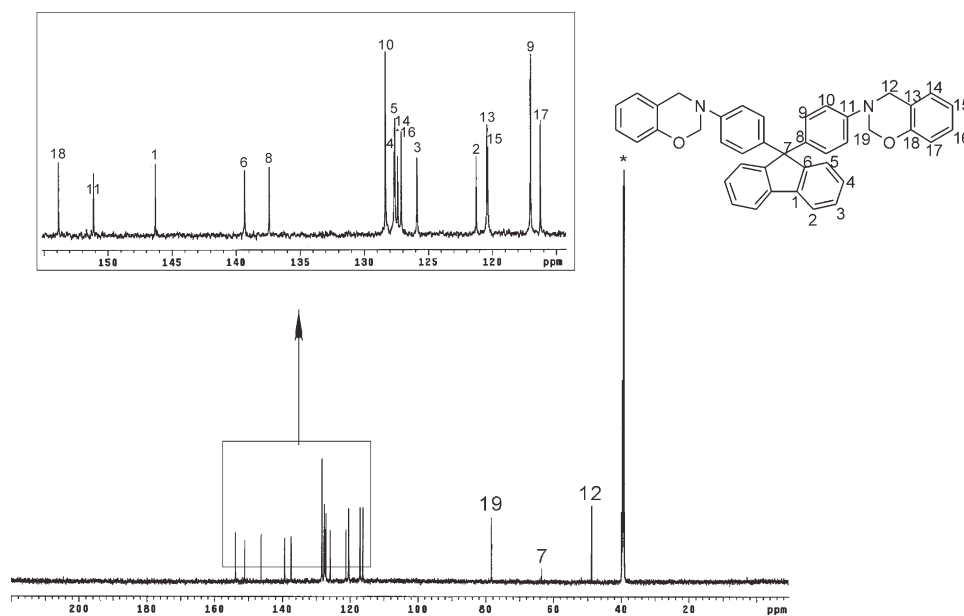
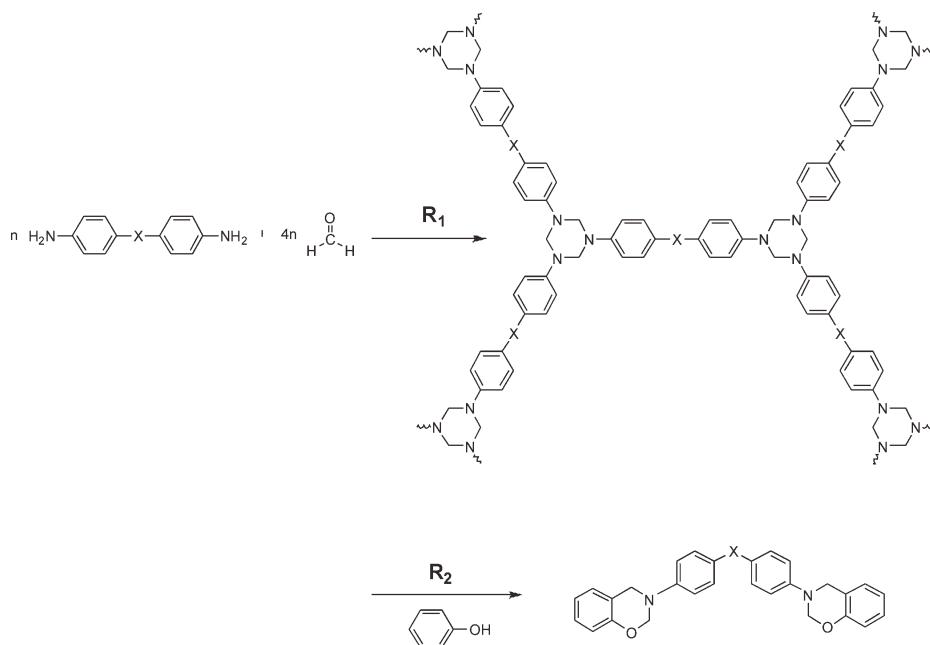


FIGURE 3 ^{13}C NMR spectrum of P-bapf-2 in $\text{DMSO-}d_6$.



SCHEME 2 Proposed reaction procedure for the preparation of a diamine-based benzoxazine. The first step involves with the formation of a triazine network (R_1) and the second step is the dissociation of the triazine network (R_2).

the solvent effect on the one-pot synthesis of **P-bapf** in this work. The **P-bapf** prepared by the one-pot procedure is referred to as **P-bapf-1**.

Table 1 lists the solvent effect on the synthesis of **P-bapf-1**. Using homosolvents, such as 1,4-dioxane (run 1), xylene (run 5), and toluene (run 9) led to some insoluble gelation. However, the degree of gelation was significantly reduced using toluene/alcohol (runs 2–4, 6–8, and 10–12) as a reaction solvent. Among these solvents, toluene/ethanol (2/1, v/v; run 11) gave the best purity and yield. Figure 4 shows the

TABLE 1 Solvent Effect on the Synthesis of P-bapf-1

Run ^a	Solvent	Reaction Status and Purity of Product ^b
1	1,4-Dioxane	Some gelatin, some impurity
2	1,4-Dioxane/methanol(2:1)	Homogeneity, poor purity
3	1,4-Dioxane/ethanol(2:1)	Homogeneity, poor purity
4	1,4-Dioxane /IPA(2:1)	Few gelatin, poor impurity
5	Xylene	Some gelatin, some impurity
6	Xylene/methanol(2:1)	Few gelatin, some impurity
7	Xylene/ethanol(2:1)	Homogeneity, some impurity
8	Xylene/IPA(2:1)	Few gelatin, some impurity
9	Toluene	Some gelatin, some impurity
10	Toluene/methanol(2:1)	Homogeneity, some impurity
11	Toluene/ethanol(2:1)	Homogeneity, little impurity
12	Toluene/IPA(2:1)	Few gelatin, some impurity

^a The reaction time is 12 h, and the reaction temperature is 80 °C for all runs.

^b ¹H NMR spectra of reaction product prepared in runs 1–12 are shown in Supporting Information Figures S3(a)–S3(l).

NMR spectrum for **P-bapf-1** prepared by run 11. The patterns shown in Figure 4 are similar to those in Figure 2, except for the small peaks at 6.4, 7.6, and 8.9 ppm. Although the purity of **P-bapf-1** is not as high as **P-bapf-2**, the ratio of the integral area of O—CH₂—N, ph—CH₂—N, and H² in **P-bapf-1** is very close to 2:2:1, suggesting a reasonable purity.

UV and PL Spectra

As the purity of **P-bapf-2** is higher than that of **P-bapf-1**, the measurements UV-vis absorption and photoluminescent data are based on **P-bapf-2**. Figure 5 shows the UV-vis absorption and photoluminescent spectra of BAPF and **P-bapf**. In the UV-vis spectra (10⁻⁵ M in ethanol), the absorption peaks are 245, 275, and 315 nm for BAPF, and 245, 260, and 315 nm for **P-bapf-2**. The spectra are nearly identical because the absorptions are determined mainly by the spin-allowed

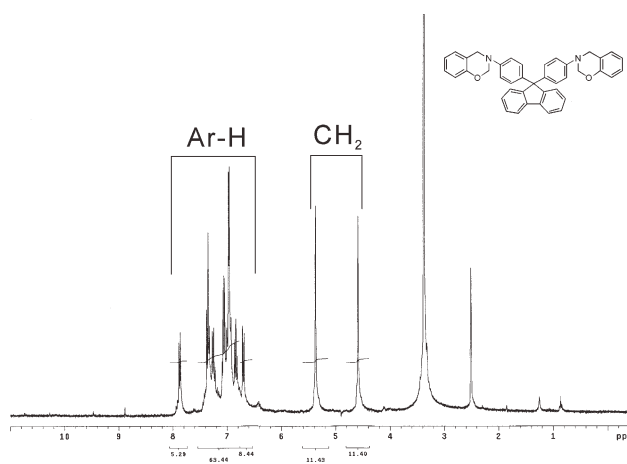


FIGURE 4 ¹H NMR spectrum of **P-bapf-1** in DMSO-*d*₆.

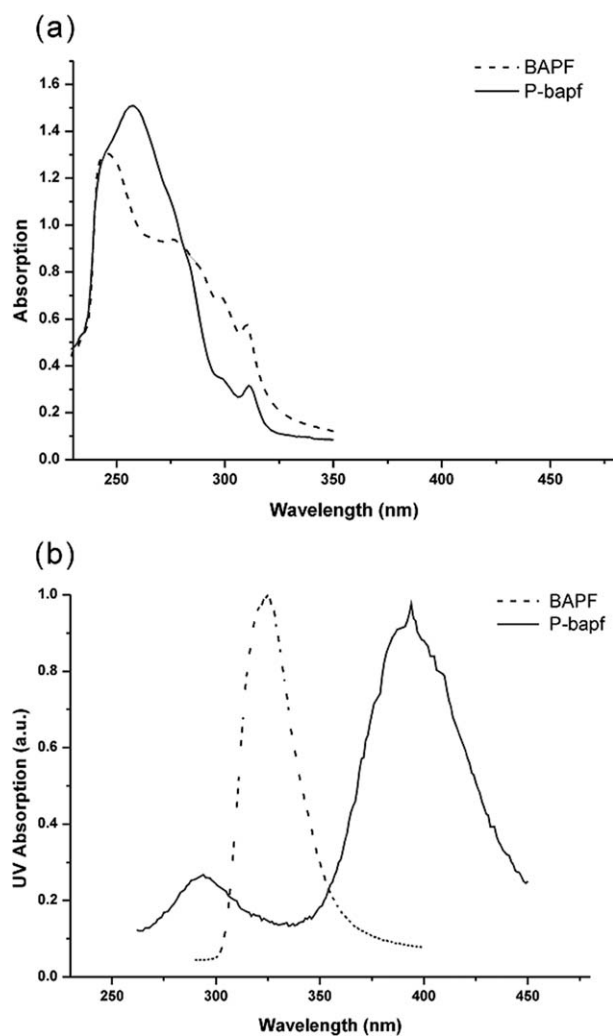


FIGURE 5 (a) UV-vis absorption and (b) PL spectra of BAPF and **P-bapf**.

π - π^* transitions involving the fluorene and phenyl structure. Compared with the absorption spectra in the range from 250 to 280 nm, the relative absorption intensity of **P-bapf** is higher than that of BAPF. The absorption is probably assigned to the absorption of the benzoxazine group. The absorption intensity of BAPF above 280 nm is higher than that of **P-bapf**. This phenomenon can likely be attributed to that the intermolecular interaction between BAPF and ethanol being stronger than it is between **P-bapf** and ethanol.^{37,38} In the PL spectra, BAPF shows an emission at 325 nm, while **P-bapf** shows an emission at 395 nm. The BAPF presented only one emission peak that belongs to the backbone of aminophenylfluorene. However, a bathochromic shift is observed in the case of **P-bapf**, indicating an enhanced conjugation due to the presence of benzoxazine moiety. The location of the maximum emission wavelength around 290 nm indicates the emission of benzoxazine chromophore, and the emission wavelength located at 395 nm may be attributed to the extended conjugated length from the nitrogen of the benzoxazine group to the phenyl ring of the fluorene.

Further study of the potential application of **P-bapf** in the blue emission is required.

DSC Thermograms of Benzoxazines

Figure 6 shows the DSC thermograms of **P-bapf-2** and **P-bapf-1**. The initial exothermic temperature of **P-bapf-2** is higher than that of **P-bapf-1**. In addition, the exothermic enthalpy of **P-bapf-2** is 246 J/g, which is larger than that (175 J/g) of **P-bapf-1**. It is known that a small amount of phenolic OH present in the precursor catalyzes the ring opening of oxazine, and consequently shifts the exothermic peak to a lower temperature. The higher initial exothermic temperature and the larger exothermic enthalpy suggest that the purity of **P-bapf-2** is better than that of **P-bapf-1**. This result is consistent with the NMR measurement.

Curing of Benzoxazines Probed by IR

Benzoxazine can be thermally cured into a cross-linked polybenzoxazine through the ring opening of the benzoxazine linkages. Figure 7 shows the IR spectra of **P-bapf** after accumulative curing for 20 min at each temperature. After curing at 220 °C, the Ar—O—C absorptions at 1039 and 1225 cm^{-1} , and the oxazine absorption 1377 cm^{-1} disappeared. The absorptions of the characteristic mode of benzene with an attached oxazine ring at 945 cm^{-1} also disappeared. In contrast, a 1,2,3-trisubstituted benzene absorption appeared at 1619 cm^{-1} . The structure of the **P-bapf** thermoset was proposed according to the IR analysis, as shown in Scheme 3. For structure-property comparisons (to be discussed later), the structure of **P-ddm** is also listed in Scheme 3. Note that **P-ddm** is a benzoxazine prepared from the condensation of diaminodiphenylmethane, phenol, and formaldehyde.³⁹

Thermal Properties of Polybenzoxazines

A dynamic mechanical analyzer was applied to measure the dynamic mechanical properties of the resultant thermosets. Figure 8 shows the DMA thermograms of the **P-bapf** thermoset. The T_g of the **P-bapf** thermoset measured by the DMA is 236 °C, which is 36 °C higher than that of the **P-ddm** thermoset (Table 2).³⁹ As shown in Scheme 3, the **P-bapf** and **P-ddm** thermosets show similar structure except for the fluorene linkages. Therefore, the higher T_g of the **P-bapf** thermoset may probably be attributed to the higher rigidity of the fluorene skeleton in the chain backbone. In addition, the T_g value of the **P-bapf** thermoset is 16 °C higher than that of the thermoset of BHPF-f, which is a benzoxazine based on 9,9-bis(4-hydroxyphenyl)fluorene/furfurylamine/formaldehyde.²⁹ The result demonstrates the high T_g characteristic of the **P-bapf** thermoset. The high T_g characteristic of fluorene structure can also be confirmed by TMA measurements. As listed in Table 2, T_g value of the **P-bapf** thermoset is 217 °C, which is 34 °C higher than the **P-ddm** thermoset. The coefficient of thermal expansion (CTE) value of **P-bapf** thermoset is 36 ppm/°C, while the CTE value of the **P-ddm** thermoset is 57 ppm/°C. The result demonstrates the dimensional stability of fluorene skeleton.

Figure 8 also shows the DMA thermogram of the **P-bapf**/CNE copolymer. Only one $\tan \delta$ peak was observed, indicating that a homogeneous copolymer was obtained. As seen in

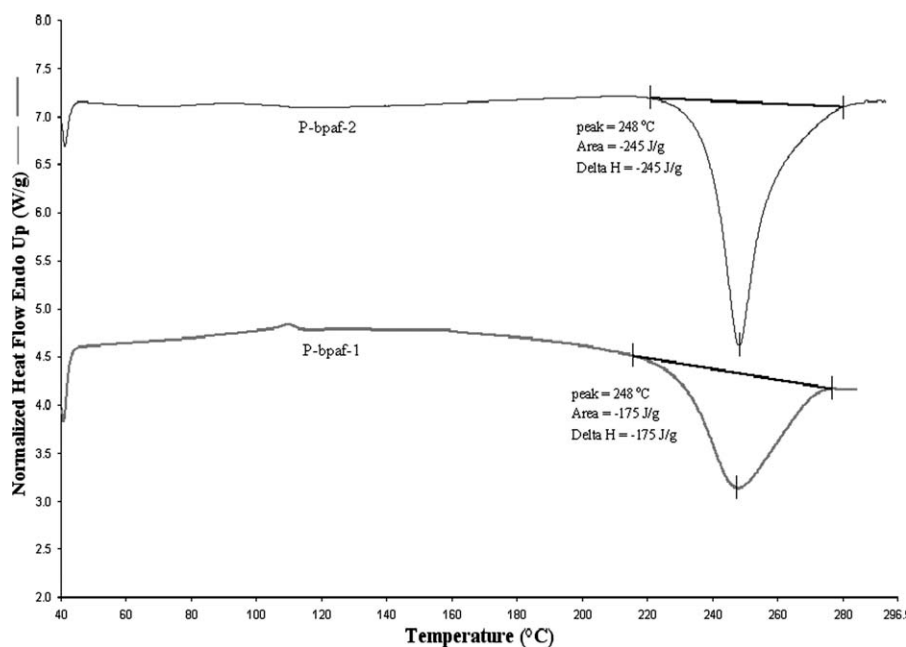


FIGURE 6 DSC thermograms of **P-bpaf-2** and **P-bpaf-1**.

Figure 8, the T_g of the **P-bapf**/CNE thermoset is as high as 260 °C, which is 24 °C higher than that of the **P-bapf** thermoset.²⁸ This indicates that the crosslinking density of the **P-bapf** thermoset was enhanced by the incorporation of CNE. It is thought that the phenolic groups, resulting from ring-opening polymerization of benzoxazine, reacted with the oxirane of CNE and thus tighten the network structure. This speculation can be confirmed by the $\tan \delta$ curves of the **P-bapf** and **P-bapf**/CNE thermosets. The height of $\tan \delta$ for the **P-bapf**/CNE thermoset is much lower than that of the **P-bapf** thermoset, confirming the higher crosslinking density of the **P-bapf**/CNE thermoset. As shown in Table 2, the T_g of the **P-bapf**/CNE copolymer is 17 °C higher than that of the

P-ddm/CNE copolymer in the DMA data, further demonstrating the high T_g characteristic of fluorene linkage. However, almost the same T_g data were detected for the **P-bapf**/CNE and **P-ddm**/CNE copolymers in the TMA measurement. Detailed analysis might be required to explain the phenomenon.

Figure 9 shows the TGA thermograms of the **P-bapf** and **P-bapf**/CNE thermosets, with the results listed in Table 2. The 5% degradation temperature of the **P-bapf** thermoset is 416 °C, which is slightly higher than that (413 °C) of the **P-ddm** thermoset. In addition, it is 82 °C higher than that of the thermoset of **BHPF-a**, which is a benzoxazine based on 9,9-bis(4-hydroxyphenyl)fluorene/aniline/formaldehyde.²⁸ The value of 416 °C is even higher than the 10% degradation

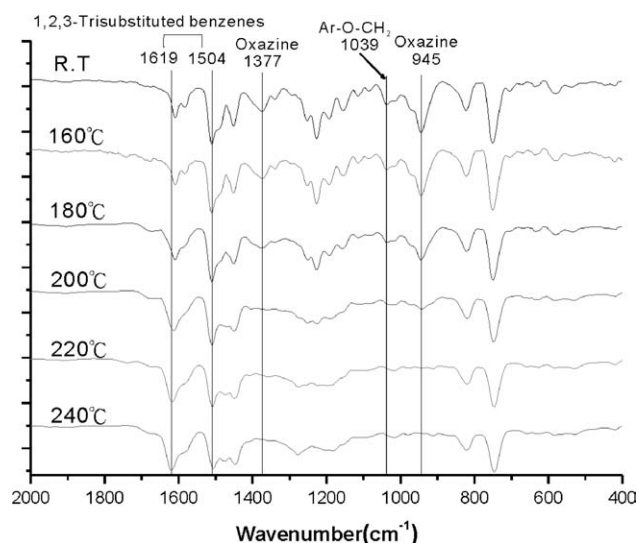
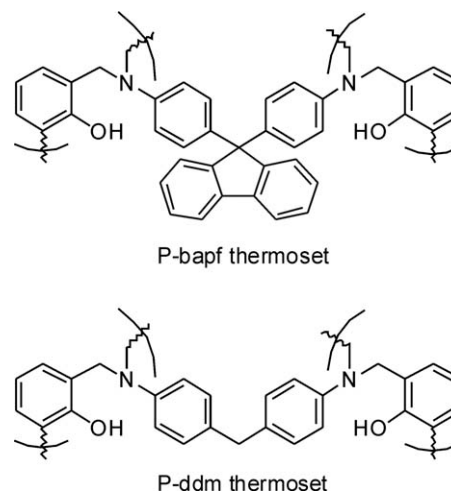


FIGURE 7 IR spectra of **P-bapf** after accumulative curing for 20 min at each temperature.



SCHEME 3 Proposed structures of **P-bapf**, **P-ddm**, **P-bapf**/CNE, and **P-ddm**/CNE thermosets.

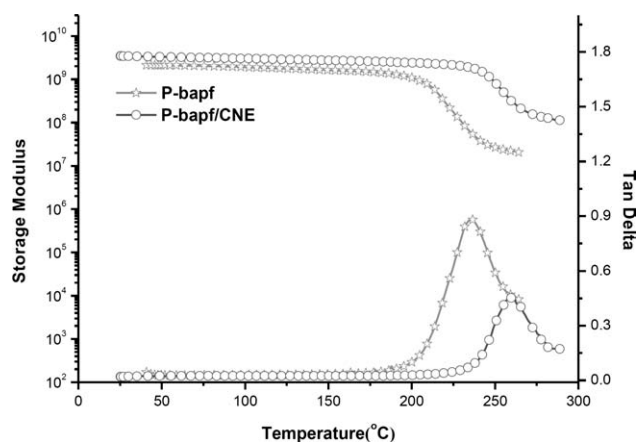


FIGURE 8 DMA thermograms of **P-bapf** and **P-bapf/CNE** thermosets.

temperature (384 °C) of **BHPF-f** thermoset.²⁹ According to the previous study, the 5% degradation temperature of biphenol/aniline/formaldehyde benzoxazine thermosets rarely exceeds 350 °C, and the release of aniline fragments is responsible for the low thermal stability of polybenzoxazines.⁴⁰ The nitrogen linkage of the **BHPF-a** thermoset is linked to a phenyl pendant, which leads to fragmentation of aniline at temperatures higher than 300 °C.⁴⁰ In contrast, as shown in Scheme 3, the nitrogen linkage in the **P-bapf** thermoset is bonded to the other repeating unit. This makes the release of aniline fragments difficult, and thus causes the **P-bapf** thermoset to be thermally more stable than the **BHPF-a** thermoset. This result demonstrates that diamine-based benzoxazine thermosets display better thermal stability than bisphenol-based benzoxazine thermosets, as has been reported in our previous work.¹⁶ As listed in Table 2, the 5% degradation temperature of the **P-bapf** thermoset in air is higher than it is in nitrogen, demonstrating the outstanding antioxidative resistance of the **P-bapf** thermoset. The char yield of the **P-bapf** thermoset in nitrogen atmosphere is 53%, which is also higher than that (46%) of the **P-ddm** thermoset. In Scheme 3, we show that the **P-bapf** and **P-ddm** thermosets have a similar structure, with the exception of the fluorene linkage. The result is consistent with the

finding that fluorene linkage effectively enhances the thermal resistance and char formation of polymers.^{25–27} As listed in Table 2, the thermal stability of the **P-bapf/CNE** thermoset is slightly lower than that of the **P-bapf** thermoset, but the 5% degradation temperature and char yield are still as high as 402 °C and 43%, respectively. However, it is known that thermal properties (e.g., T_g , decomposition temperature) of all thermosets are pretty much dependent on extent of cross-linking. The thermal property data in Table 2 are not absolute as no optimal curing procedure was researched in this work.

Refractive Index

Fluorene-containing polymers, such as polyimides,^{25,41} polyether,²⁷ poly(ether ether ketone),⁴² have been proven to exhibit high refractive indices due to their high aromatic contents. Figure 10 shows the refractive index of the **P-bapf** thermoset. The refractive index at 589 nm is 1.70, which is much higher than that (1.58) of the bis(3-furfuryl-3,4-dihydro-2H-1,3-benzoxazinyl)isopropane thermoset.⁴³ The value is also higher than that (1.65) of **BHPF-f**²⁹ and that (1.646) of fluorene-containing poly(ether ether ketone).⁴² The result demonstrates the high-refractive-index characteristic of the **P-bapf** thermoset. The high refractive-index characteristic makes **P-bapf** thermoset a potential candidate in antireflective coating.

CONCLUSIONS

A 9,9-bis(4-aminophenyl)fluorene/phenol/formaldehyde-based benzoxazine, **P-bapf**, was successfully prepared by a one-pot and a two-pot approach, respectively. We found that the reaction solvent had a profound effect on the purity and yield of benzoxazine synthesis in the one-pot approach. Using toluene/ethanol (2/1, v/v) as a cosolvent leads to the best purity and yield. We also found that benzoxazine **P-bapf** prepared by the two-pot approach has a better purity, although the approach is relatively time consuming and more expensive in the raw materials. After curing, the **P-bapf** thermoset exhibits higher T_g (236 °C) than the **P-ddm** thermoset (200 °C). This result may probably be attributed to the higher rigidity of the fluorene skeleton as the **P-bapf** and **P-ddm** thermosets have similar structures except for the fluorene linkage. Compared with the bisphenol-based

TABLE 2 Thermal Properties of the **P-bapf** and **P-bapf/CNE** Thermosets

Thermoset Based on	E' (GPa) ^a	T_g DMA (°C) ^b	T_g TMA (°C) ^c	CTE (ppm/°C) ^d	T_d (N ₂ ; °C) ^e	T_d (air; °C) ^f	Char Yield (wt %) ^g	Char Yield (wt %) ^h
P-bapf	2.2	236	217	36	416	431	53	22
P-bapf/CNE	3.3	260	223	49	402	409	43	4.0
P-ddm ⁱ	2.28	200	183	57	413	–	46	–
P-ddm/CNE ⁱ	3.19	243	225	54	406	–	40	–

^a Storage modulus (E') at 50 °C.

^b Measured by DMA at a heating rate of 5 °C/min.

^c Measured by TMA at a heating rate of 5 °C/min.

^d Coefficient of thermal expansion before T_g .

^e Five percentage degradation temperature in a nitrogen atmosphere.

^f Five percentage degradation temperature in air.

^g Residual weight percentage at 800 °C in nitrogen.

^h Residual weight percentage at 800 °C in air.

ⁱ Data from reference.³⁹

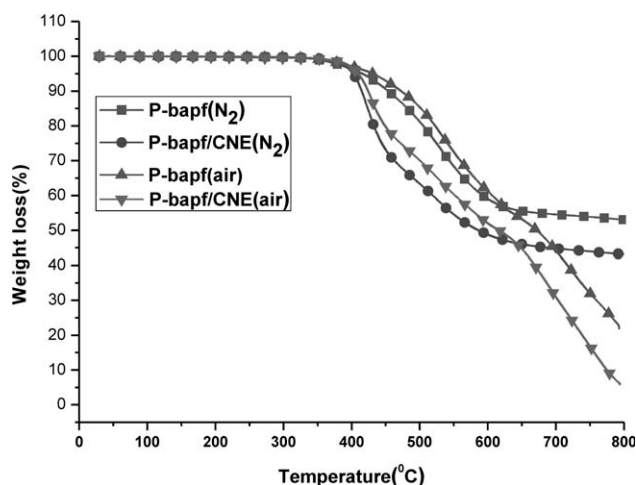


FIGURE 9 TGA thermograms of the P-bapf and P-bapf/CNE thermosets in (a) N₂ and (b) air.

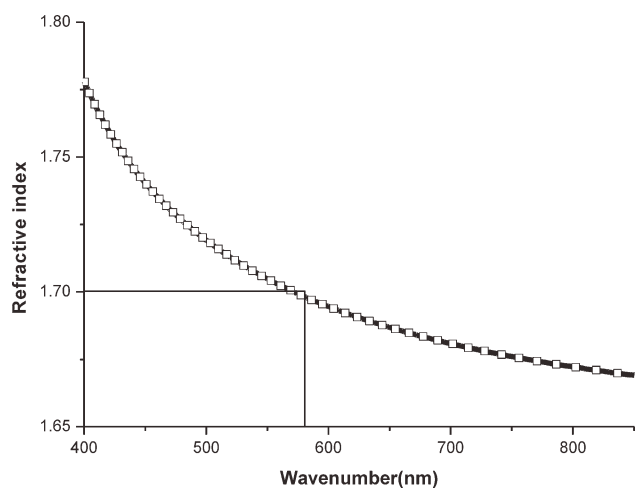


FIGURE 10 Refractive index of the P-bapf thermoset at various wavenumbers.

BHPF-a thermoset, the diamine-based P-bapf thermoset displays much better thermal stability and a higher refractive index. The combination of high T_g , good thermal stability, higher char yield, and a high refractive index makes the P-bapf thermoset attractive in electronic applications.

The authors thank the National Science Council of the Republic of China, Taiwan, for financial support. Partial sponsorship by the Green Chemistry Project (NCHU), funded by the Ministry of Education, is also gratefully acknowledged.

REFERENCES AND NOTES

- 1 Ghosh, N. N.; Kiskan, B.; Yagci, Y. *Prog. Polym. Sci.* **2007**, *32*, 1344–1391.
- 2 Ning, X.; Ishida, H. *J. Polym. Sci. Part A: Polym. Chem.* **1994**, *32*, 1121–1129.
- 3 Wang, C.-F.; Su, Y.-C.; Kuo, S.-W.; Huang, C.-F.; Sheen, Y.-C.; Chang, F.-C. *Angew. Chem. Int. Ed.* **2006**, *45*, 2248–2251.

- 4 Chernykh, A.; Agag, T.; Ishida, H. *Macromolecules* **2009**, *42*, 5121–5127.
- 5 Dogan Demir, K.; Kiskan, B.; Yagci, Y. *Macromolecules* **2011**, *44*, 1801–1807.
- 6 Liu, Y.-L.; Chou, C.-I. *J. Polym. Sci. Part A: Polym. Chem.* **2005**, *43*, 5267–5282.
- 7 Agag, T.; Takeichi, T. *Macromolecules* **2003**, *36*, 6010–6017.
- 8 Agag, T.; Takeichi, T. *Macromolecules* **2001**, *34*, 7257–7263.
- 9 Liu, Y.-L.; Yu, J.-M. *J. Polym. Sci. Part A: Polym. Chem.* **2006**, *44*, 1890–1899.
- 10 Andreu, R.; Reina, J. A.; Ronda, J. C. *J. Polym. Sci. Part A: Polym. Chem.* **2008**, *46*, 6091–6101.
- 11 Jin, L.; Agag, T.; Yagci, Y.; Ishida, H. *Macromolecules* **2011**, *44*, 767–772.
- 12 Agag, T.; Arza, C. R.; Maurer, F. H. J.; Ishida, H. *Macromolecules* **2010**, *43*, 2748–2758.
- 13 Agag, T.; Jin, L.; Ishida, H. *Polymer* **2009**, *50*, 5940–5944.
- 14 Baqar, M.; Agag, T.; Ishida, H.; Qutubuddin, S. *Polymer* **2011**, *52*, 307–317.
- 15 Chernykh, A.; Agag, T.; Ishida, H. *Polymer* **2009**, *50*, 382–390.
- 16 Lin, C. H.; Chang, S. L.; Hsieh, C. W.; Lee, H. H. *Polymer* **2008**, *49*, 1220–1229.
- 17 Lin, C. H.; Chang, S. L.; Lee, H. H.; Chang, H. C.; Hwang, K. Y.; Tu, A. P.; Su, W. C. *J. Polym. Sci. Part A: Polym. Chem.* **2008**, *46*, 4970–4983.
- 18 Andreu, R.; Ronda, J. C. *Synth. Commun.* **2008**, *38*, 2316–2329.
- 19 Oie, H.; Sudo, A.; Endo, T. *J. Polym. Sci. Part A: Polym. Chem.* **2011**, *49*, 3174–3183.
- 20 Wu, X.; Zhou, Y.; Liu, S.-Z.; Guo, Y.-N.; Qiu, J.-J.; Liu, C.-M. *Polymer* **2011**, *52*, 1004–1012.
- 21 Wu, X.; Liu, S.-Z.; Tian, D.-T.; Qiu, J.-J.; Liu, C.-M. *Polymer* **2011**, *52*, 4235–4245.
- 22 Abbel, R.; Schenning, A. P. H. J.; Meijer, E. W. *J. Polym. Sci. Part A: Polym. Chem.* **2009**, *47*, 4215–4233.
- 23 Leni, A. *Prog. Polym. Sci.* **2003**, *28*, 875–962.
- 24 Kim, D. Y.; Cho, H. N.; Kim, C. Y. *Prog. Polym. Sci.* **2000**, *25*, 1089–1139.
- 25 Terraza, C. A.; Liu, J.-G.; Nakamura, Y.; Shibasaki, Y.; Ando, S.; Ueda, M. *J. Polym. Sci. Part A: Polym. Chem.* **2008**, *46*, 1510–1520.
- 26 Seesukphronrarak, S.; Kawasaki, S.; Kobori, K.; Takata, T. *J. Polym. Sci. Part A: Polym. Chem.* **2008**, *46*, 2549–2556.
- 27 Seesukphronrarak, S.; Kawasaki, S.; Kobori, K.; Takata, T. *J. Polym. Sci. Part A: Polym. Chem.* **2007**, *45*, 3073–3082.
- 28 Wang, J.; Wu, M.-Q.; Liu, W.-B.; Yang, S.-W.; Bai, J.-W.; Ding, Q.-Q.; Li, Y. *Eur. Polym. J.* **2010**, *46*, 1024–1031.
- 29 Liu, Y.-L.; Chang, C.-Y.; Hsu, C.-Y.; Tseng, M.-C.; Chou, C.-I. *J. Polym. Sci. Part A: Polym. Chem.* **2010**, *48*, 4020–4026.
- 30 Maya, E. M.; Muñoz, D. M.; Lozano, A. E.; de Abajo, J.; de la Campa, J. G. *J. Polym. Sci. Part A: Polym. Chem.* **2008**, *46*, 8170–8178.
- 31 Wang, C.; Zhao, X.; Li, G.; Jiang, J. *Polym. Degrad. Stab.* **2009**, *94*, 1746–1753.
- 32 Guo, X.; Fang, J.; Watari, T.; Tanaka, K.; Kita, H.; Okamoto, K.-I. *Macromolecules* **2002**, *35*, 6707–6713.
- 33 Kaya, İ.; Yildirim, M.; Aydın, A.; Şenol, D. *React. Funct. Polym.* **2010**, *70*, 815–826.

- 34** Liu, W.; Qiu, Q.; Wang, J.; Huo, Z.; Sun, H. *Polymer* **2008**, *49*, 4399–4405.
- 35** Brunovska, Z.; Liu, J. P.; Ishida, H. *Macromol. Chem. Phys.* **1999**, *200*, 1745–1752.
- 36** Lin, C. H.; Chang, S. L.; Shen, T. Y.; Shih, Y. S.; Lin, H. T.; Wang, C. F. *Polym. Chem.* **2012**, DOI: 10.1039/c2py00449f.
- 37** Dey, J. K.; Dogra, S. K. *Chem. Phys.* **1990**, *143*, 97–107.
- 38** El-Sayed, M.; Blaudeck, T.; Cichos, F.; Spange, S. *J. Photochem. Photobiol. A: Chem.* **2007**, *185*, 44–50.
- 39** Chang, S. L.; Lin, C. H. *J. Polym. Sci. Part A: Polym. Chem.* **2010**, *48*, 2430–2437.
- 40** Hemvichian, K.; Ishida, H. *Polymer* **2002**, *43*, 4391–4402.
- 41** Hsiao, S.-H.; Li, C.-T. *J. Polym. Sci. Part A: Polym. Chem.* **1999**, *37*, 1403–1412.
- 42** Kawasaki, S.; Yamada, M.; Kobori, K.; Jin, F.; Kondo, Y.; Hayashi, H.; Suzuki, Y.; Takata, T. *Macromolecules* **2007**, *40*, 5284–5289.
- 43** Tseng, M.-C.; Liu, Y.-L. *Polymer* **2010**, *51*, 5567–5575.